Polyhedral Flexibility in the Sulfido-Capped Cluster $H_2Ru_3(CO)_9(\mu_3\text{-}S)$ on Reaction with 2-(Diphenylphosphino)thioanisole (PS) and Reversible Tripodal Rotation of the Chelated PS ligand in $H_2Ru_3(CO)_7(\kappa^2\text{-}PS)(\mu_3\text{-}S)$

Darrell D. Mayberry, Vladimir N. Nesterov, and Michael G. Richmond*

Department of Chemistry, University of North Texas, Denton, Texas 76203, United States.

ABSTRACT: Treatment of the tetrahedral cluster $H_2Ru_3(CO)_9(\mu_3\text{-}S)$ (**1**) with 2-(diphenylphosphino)thioanisole (PS) furnishes the cluster $H_2Ru_3(CO)_7(\kappa^2\text{-}PS)(\mu_3\text{-}S)$ (**2**). Cluster **2**, which exhibits a chelated thiophosphine ligand (κ^2-PS), exists as a pair of diastereomers with K_{eq} = 1.55 at 298 K that differ in their disposition of ligands at the Ru(CO)(κ^2-PS) center. The PS ligand occupies the equatorial sites (P_{eq}, S_{eq}) in the kinetic isomer and axial and equatorial sites (P_{ax}, S_{eq}) in the thermodynamically favored species. The solid-state structure of the kinetic isomer of **2** has been established by X-ray diffraction analysis, and the reversible first-order kinetics to equilibrium have been measured experimentally by NMR spectroscopy and HPLC over the temperature range 293-323 K. The substitution reaction involving **1** and the isomerization of the PS ligand in **2** were investigated by DFT calculations. The computational results support a phosphine-induced expansion of the cluster polyhedron that is triggered by the associative addition of the PS donor to **1**. The vertex opening in **1** is selective and leads to the cleavage of a hydride-bridged Ru-Ru bond to give the phosphine-substituted cluster $H_2Ru_3(CO)_9(\kappa^1\text{-}PS)(\mu_3\text{-}S)$ as the initial adduct. Chelation of the pendant MeS moiety follows with a loss of CO to give the kinetic substitution product $H_2Ru_3(CO)_7(\kappa^2\text{-}P_{eq}, S_{eq})(\mu_3\text{-}S)$ (**2**). The observed isomerization of the PS ligand in **2** is best explained by a tripodal rotation of the CO and PS groups at the Ru(CO)(κ^2-PS) center that is preceded by a regiospecific migration of one of the edge-bridging hydrides to the non-hydride-bridged Ru-Ru bond in **2**.

Introduction

The coordination chemistry and reactivity of hemilabile ligands at mononuclear metal compounds have been studied for a longer time and more extensively compared to polynuclear clusters. The reactivity of cluster-bound hemilabile ligands remains a relatively unexplored area of chemistry, and before any reactivity generalizations and predictions can be made with a trusted degree of certainty, answers on the preferred binding mode, stereochemical preferences, and dynamical properties of such ligands at different metal clusters are required.

Typically, heterobidentate hemilabile donors react with metal clusters to give chelated or bridged products depending on the nature of the ligand and the energetics associated with the different product isomers, and this phenomenon was first described by Nordlander and co-workers in 2001 for the reaction of the triosmium cluster 1,2-$Os_3(CO)_{10}(MeCN)_2$ with the hemilabile donor (2-methylthioethyl)diphenylphosphine (PS').[1] The bridged cluster $Os_3(CO)_{10}(\mu\text{-}PS')$ is formed as a kinetic product of substitution that undergoes a slow, non-dissociative isomerization to the thermodynamically favored chelated cluster $Os_3(CO)_{10}(\kappa^2\text{-}PS')$ (Scheme 1).[2] Here the thiomethyl moiety promotes an in-plane migration of ligands about the Os-Os bond by changing from a 2e to 4e donor that enables the coordination of adjacent metal centers. Other reports on the reaction of PS, PSP, and PSSP donors with metal clusters have since appeared,[3] but the total number of examples is small compared to the mononuclear studies published to date.

Scheme 1. Isomerization of the PS' ligand in $Os_3(CO)_{10}[(MeSCH_2CH_2)PPh_2]$

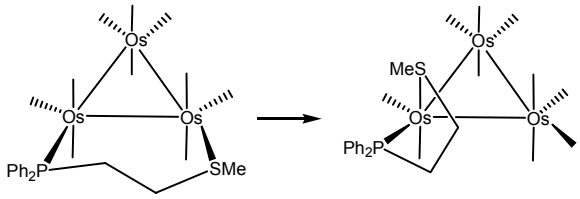

We recently published a report on the catalytic hydrogenation of tiglic acid using the diphosphine-substituted clusters $H_2Ru_3(CO)_7$(Walphos)(μ_3-S) [where Walphos = chiral 2'-(diphenylphosphino)phenyl]ferrocenyl}ethyldi[3,5-bis(trifluoromethyl)phenyl]phosphine].[4] The $H_2Ru_3(CO)_7$(Walphos)(μ_3-S) cluster exists as a pair of Walphos-bridged diastereomers where the phosphine ligand bridges one of the hydride-bridged Ru-Ru bonds through the axial and equatorial sites. Earlier Bruce and co-workers reported the synthesis of several diphosphine-substituted $H_2Ru_3(CO)_7(\mu\text{-}PP)(\mu_3\text{-}S)$ clusters using reagent-assisted activation of **1**.[5] The products contain a bridging PP ligand that occupies equatorial sites at the hydride-bridged Ru-Ru bond. Apart from these two studies,[4,5] the direct reaction of **1** with bidentate donors is silent; although we note that both chelated and bridged diphosphine-substituted clusters $H_2Ru_3(CO)_7(PP)(\mu_3\text{-}S)$ have been indirectly synthesized from

the precursors $Ru_3(CO)_{10}(\mu$-PP) and $HRu_3(CO)_8(PP)(\mu$-SR) in the presence of H_2S and H_2, respectively.[6] Apart from common diphosphine donors, a chemical void exists concerning the study of **1** with asymmetric bidentate donors, of which, the hemilabile variety is long overdue for investigation. Herein we present our results on the synthesis of $H_2Ru_3(CO)_7(\kappa^2$-PS)(μ_3-S), which is produced in high yield from the reaction of the hemilabile donor 2-(diphenylphosphino)thioanisole (PS) with the sulfido-capped cluster $H_2Ru_3(CO)_9(\mu_3$-S). Cluster **2** is the first hemilabile-substituted cluster based on **1** and it is also the first cluster whose PS ligand exhibits a reversible tripodal rotation that serves to equilibrate the PS moiety at the chelated ruthenium center from the kinetic stereoisomer with a P_{eq}, S_{eq} disposition to the thermodynamically favored stereoisomer with P_{ax}, S_{eq} orientation.

Results and Discussion

1. Syntheses and Characterization of $H_2Ru_3(CO)_7(\kappa^2$-PS)(μ_3-S). Treatment of an equimolar mixture of $H_2Ru_3(CO)_9(\mu_3$-S) (**1**) and 2-(diphenylphosphino)thioanisole (PS) with Me_3NO (2 equivs.) in CH_2Cl_2 at room temperature gives a pair of diastereomers that possess a chelated PS ligand and exhibit the formula $H_2Ru_3(CO)_7(\kappa^2$-PS)(μ_3-S) (**2**). NMR analysis after 1 hr confirms the presence of an 8:1 mixture of products. This ratio decreased to 1:1 for those reactions that were stirred overnight and yielded a limiting K_{eq} value of 1.55 for samples that were heated in a thermostated bath at 298 K for 2 weeks. These data support the existence of a dynamic equilibrium between the two diastereomers that involves the formation of a kinetic isomer that undergoes a slow conversion to its thermodynamic counterpart.

Our attempts to separate the two products by traditional column chromatography were unsuccessful, so we next examined preparative HPLC using a commercially available reverse-phase C_{18} column. The two products could be separated using a binary eluent composed of MeCN/H_2O (9:1), after which the isolated products equilibrated consistent with our premise of a dynamic equilibrium between the two products. These data are illustrated in Figure S1.

We were able to grow single crystals of one of the products for X-ray diffraction analysis from an equilibrated mixture containing cluster **2**. Figure 1 shows the solid-state structure of the PS-chelated cluster where the PS ligand occupies the equatorial sites at the Ru(1) center that is flanked by both hydrides.[7] To our knowledge this is the first structure based on cluster **1** that contains an ancillary PS ligand. No examples of a cluster with a bridging PS ligand are known, and this may reflect the relatively small bite angle of the ligand that prefers to bind one metal as opposed to bridging two metal centers.[8] The cluster core in $H_2Ru_3(CO)_7(\kappa^2$-P_{eq},S_{eq})(μ_3-S) (**2**-P_{eq}, S_{eq}) consists of an isosceles triangle of ruthenium atoms whose metallic face is capped by the S(1) group. Chelation of the PS ligand in **2**-P_{eq},S_{eq} does not adversely perturb the cluster polyhedron as the mean Ru-Ru and Ru-S(1) distances of 2.8321 and 2.3704 Å parallel the mean Ru-Ru and Ru-S distances of 2.840 and 2.364 Å reported by Adams and Katahira for the parent cluster **1**.[9] The two hydrides lie below the metallic plane opposite the sulfido cap, and the P(1) atom lies trans to the hydride that spans the Ru(1)-Ru(2) vector [P(1)-Ru(1)-H(a) = 173(2)°] and cis to the hydride associated with the Ru(1)-Ru(3) bond [P(1)-Ru(1)-H = 93(1)°]. The Ru(1)-S(2) bond distance of 2.3293(8) is comparable to the mean Ru-S(1) distance, and the sum of the angles about the S(2) atom is ca. 319°, confirming the pyramidal geometry at the thioether moiety. Fast sulfur inversion has been reported for a series of mononuclear ruthenium compounds with coordinated thioethers.[10] Out of the two possible orientations available to the C(26) methyl group in **2**-P_{eq},S_{eq}, the one that places the C(26) group distal to the capping sulfido ligand and proximal to the bridging hydride H(a) is experimentally found based on the S(1)-Ru(1)-S(2)-C(26) torsion angle of 149.3(3)°.

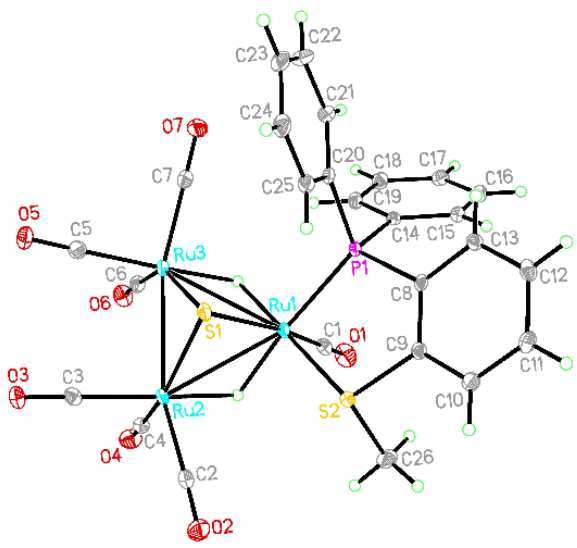

Figure 1. Molecular structure of $H_2Ru_3(CO)_7(\kappa^2$-P_{eq}, S_{eq})(μ_3-S). Thermal ellipsoids are drawn at the 50% probability level. Selected bond distances (Å) and angles (deg): Ru(1)-Ru(2) = 2.8785(3); Ru(1)-Ru(3) = 2.8733(3); Ru(2)-Ru(3) = 2.7445(4); Ru(1)-S(2) = 2.3293(8); Ru(1)-P(1) = 2.2874(8); P(1)-Ru(1)-S(2) = 86.49(3); P(1)-Ru(1)-H(A) = 173(2); P(1)-Ru(1)-H = 93(1).

The identity of the products in the reaction mixture was ascertained by ^{1}H NMR spectroscopy. Both species exhibit a distinct pair of bridging hydrides that comprise the AB portion of an ABX spin system and whose geminal coupling to the ancillary phosphine facilitates the stereochemical assignment of the phosphine moiety relative to the hydrides. The kinetic product displays a pair of doublet of doublets (dd) centered at δ -20.11 and -17.26 where the small 1.8 Hz splitting observed derives from hydride-hydride coupling, as verified by ^{1}H COSY.[11] The resonance at δ -17.26 exhibits a large $^2J_{PH}$ coupling of 34.0 Hz in full support for a trans orientation of the phosphine to one of the hydrides.[12] Of the four different equatorial sites that are trans to a hydride in the cluster polyhedron, the locus for the phosphine must also be situated cis to the second hydride in order to account for the $^2J_{PH}$ coupling of 9.5 Hz. The site of phosphine substitution consistent with these stereochemical requirements is at one of the two equatorial sites at the ruthenium atom that is flanked by both bridging hydrides. Since the site of MeS substitution (equatorial versus axial) could not be unequivocally established by NMR, we investigated the site preference by DFT. The chelated isomer with a P_{eq}, S_{eq} ligand disposition was determined to be 2.0 kcal/mol more stable than

the alternative stereoisomer possessing a P_{eq}, S_{ax} orientation. The NMR and DFT data, taken collectively, are consistent with the solid-state structure that may be confidently assigned as the kinetic product of ligand substitution. The thermodynamics for the formation of the two chelated products were evaluated by DFT according to the stoichiometry: cluster **1** + PS → cluster **2** + 2CO. The reaction is endergonic by >12 kcal/mol and entropically driven by the release of CO (two equivs).

The thermodynamically favored isomer exhibits an axial phosphine based on the recorded $^2J_{PH}$ values of 8.3 and 11.3 Hz. The magnitude of these couplings requires the proximal location of the phosphine relative to the two hydrides, a condition that mandates an axial disposition of the phosphine moiety. The magnitude of the $^2J_{PH}$ values in the thermodynamic isomer $H_2Ru_3(CO)_7(\kappa^2\text{-}P_{ax}, S_{eq})(\mu_3\text{-}S)$ is similar to the 10 Hz value reported by Stone *et al.* for the monophosphine-substituted cluster $H_2Ru_3(CO)_8(PPh_3)(\mu_3\text{-}S)$ that reveals a hydride doublet at δ -18.31 ($^2J_{PH}$ = 10.0 Hz) in the ^{1}H NMR spectrum.[13] The observed hydride splitting in $H_2Ru_3(CO)_8(PPh_3)(\mu_3\text{-}S)$ is consistent with an axial PPh_3 group and a product having C_s symmetry. Accordingly, the ^{1}H NMR spectrum of $H_2Ru_3(CO)_7(\kappa^2\text{-}P_{ax}, S_{eq})(\mu_3\text{-}S)$ supports the axial coordination of the phosphine at the ruthenium atom bound by both edge-bridging hydrides. A P_{ax} orientation, in turn, requires the equatorial disposition of the MeS ligand and allows us to posit with confidence $H_2Ru_3(CO)_7(\kappa^2\text{-}P_{ax}, S_{eq})(\mu_3\text{-}S)$ as the thermodynamic isomer in the reaction of **1** with PS. Scheme 2 shows the course of the reaction as a function of the two products and their geminal coupling constants.

Scheme 2. Diastereomers **2**-(P_{eq}, S_{eq}) and **2**-(P_{ax}, S_{eq}) produced from the reaction of **1** with PS.

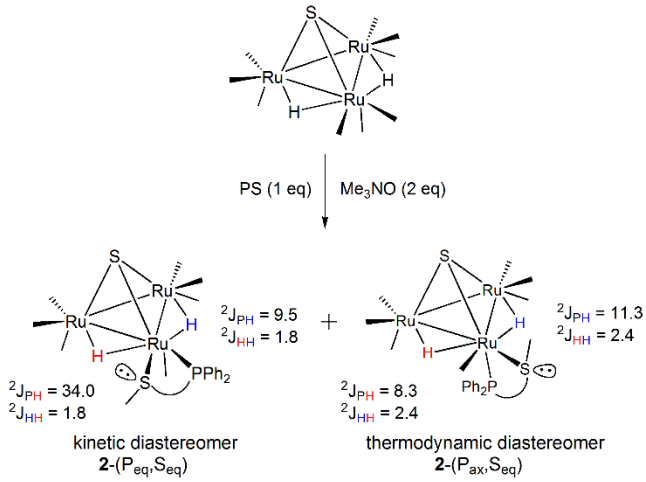

We have also examined other synthetic methods for the reaction of **1** with PS in order to study the effect different conditions have, if any, on the ligand regiochemistry in the substituted product. We prepared the MeCN-substituted cluster $H_2Ru_3(CO)_8(MeCN)(\mu_3\text{-}S)$ *in situ* from **1** and Me_3NO (1 equiv) in MeCN and studied the substitution reaction with PS. The replacement of a CO ligand in a binary metal carbonyl by an MeCN group gives, as a rule of thumb, activated precursors that exhibit enhanced chemical reactivity in ligand substitution reactions vis-á-vis the parent carbonyl.[14] The IR spectrum of $H_2Ru_3(CO)_8(MeCN)(\mu_3\text{-}S)$ reveals ν(CO) bands at 2085m, 2053v, 2047s, and 2003s cm^{-1} similar in nature to the osmium derivative $H_2Os_3(CO)_8(MeCN)(\mu_3\text{-}S)$ prepared by Deeming and Hogarth.[15] $H_2Ru_3(CO)_8(MeCN)(\mu_3\text{-}S)$ reacts with PS (1 equiv) at room temperature to give an intermediate monophosphine-substituted cluster consistent with the formula $H_2Ru_3(CO)_8(\kappa^P\text{-}PS)(\mu_3\text{-}S)$. The observation of the phosphine-substituted cluster as the initial product from the addition of the PS donor to cluster **1** establishes the phosphine moiety, as opposed to the sulfur moiety, as the kinetically preferred donor. The ^{1}H NMR spectrum reveals a hydride doublet at δ -18.28 ($^2J_{PH}$ = 9.5 Hz) akin to that reported for $H_2Ru_3(CO)_8(PPh_3)(\mu_3\text{-}S)$.[13] Our Ru_3 intermediate is not stable and loses CO over several hours to furnish cluster **2** as a mixture of diastereomers whose composition depends on the resident time in solution. Treatment of $H_2Ru_3(CO)_8(\kappa^P\text{-}PS)(\mu_3\text{-}S)$ with added Me_3NO promotes the rapid chelation of the MeS group and formation of cluster **2**. We also attempted to prepare the bis(acetonitrile) cluster $H_2Ru_3(CO)_7(MeCN)_2(\mu_3\text{-}S)$ from **1** using two equivalents of Me_3NO. This experiment was conducted in a mixture of $CD_3CN/CDCl_3$ and was monitored by ^{1}H NMR spectroscopy. We observed $H_2Ru_3(CO)_8(CD_3CN)(\mu_3\text{-}S)$ after **1** hr, along with a small amount of cluster **3**, leading us to conclude that the formation of the bis(acetonitrile) cluster is sluggish under these conditions; no further effort was expended in the preparation of this derivative.

The lability of the coordinated MeCN ligand in $H_2Ru_3(CO)_8(MeCN)(\mu_3\text{-}S)$ was confirmed by the crystals obtained from a stock solution of the cluster in CH_2Cl_2 that was allowed to sit for several days under argon in a storage vessel. Dark orange crystals were deposited after one week and whose identity was subsequently established by single-crystal X-ray diffraction analysis. The solved structure corresponds to the cyclic trimer $[H_2Ru_3(CO)_8(\mu_4\text{-}S)]_3{\cdot}CH_2Cl_2$ (**3**) that is a pseudopolymorph of the trimeric cluster reported by Adams and co-workers.[16] Figure 2 shows the thermal ellipsoid plot of the molecular structure of **3**. The bond distances and angles in **3** are reported in the SI document. The isolation of **3** provides strong support for a weakly bound, labile MeCN ligand in $H_2Ru_3(CO)_8(MeCN)(\mu_3\text{-}S)$. Dissociation of MeCN generates the unsaturated cluster $H_2Ru_3(CO)_8(\mu_3\text{-}S)$ which trimerizes in a head-to-tail coupling of the individual Ru_3 units. The cluster aggregation is driven by the capture of the unsaturated ruthenium atom using the capping sulfido moiety of a second cluster. The linking of three Ru_3 units in this process is accompanied by a $\mu_3 \rightarrow \mu_4$ change in the sulfido groups as each sulfido ligand transforms from a 4e to 6e donor.

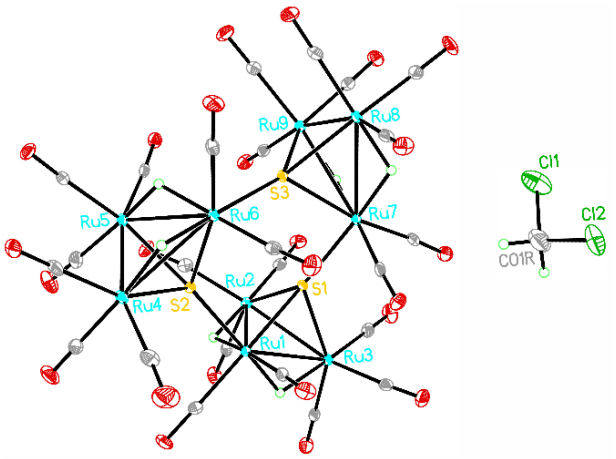

Figure 2. Molecular structure of $[H_2Ru_3(CO)_8(\mu_4\text{-}S)]_3 \cdot CH_2Cl_2$ (**3**). Thermal ellipsoids are drawn at the 50% probability level

We also conducted a control experiment involving **1** and PS (1 equiv), and this reaction was performed at room temperature in the absence of external activation. Surprisingly, the PS donor adds to **1** to furnish $H_2Ru_3(CO)_8(\kappa^P\text{-}PS)(\mu_3\text{-}S)$, the same intermediate recorded in the reaction between $H_2Ru_3(CO)_8(MeCN)(\mu_3\text{-}S)$ and PS. The concentration of the monosubstituted κ^P product remained low (<20%) in those reactions monitored by NMR; this same species functions as an indispensable precursor in the ensuing MeS chelation/decarbonylation steps that ultimately give $H_2Ru_3(CO)_7(\kappa^2\text{-}PS)(\mu_3\text{-}S)$ (**2**) along with liberated CO. Stirring an equimolar samples of **1** and PS at room temperature overnight revealed a 1:6 mixture of $H_2Ru_3(CO)_8(\kappa^P\text{-}PS)(\mu_3\text{-}S)$: $H_2Ru_3(CO)_7(\kappa^2\text{-}PS)(\mu_3\text{-}S)$ by ^1H NMR, with the ratio of the diastereomer products **2**-(P_{eq}, S_{eq}):**2**-(P_{ax}, S_{eq}) determined to be 1:1 at this point. Complete conversion to products and equilibrium (K_{eq} = 1.55) was achieved after 1 week at room temperature. Scheme 3 illustrates the course of this reaction in terms of the species that have been observed spectroscopically.

Scheme 3. Stereochemistry in the phosphine-substituted intermediate and chelated products from the reaction of **1** and PS.

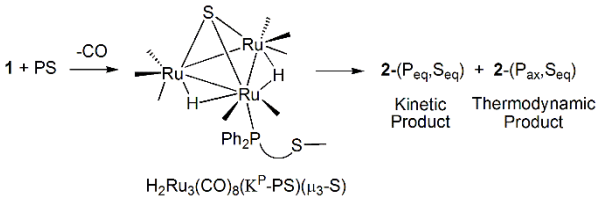

II. DFT Evaluation of the Isomeric $H_2Ru_3(CO)_7(PS)(\mu_3\text{-}S)$ Clusters. Electronic structure calculations were performed on **2** to determine if we could accurately reproduce the energy difference between the two products with respect to the experimental value, as assessed through the value of K_{eq} measured at equilibrium. The second area of interest was the computational evaluation of the relative energies of alternative isomers as a function of coordination mode exhibited by the PS ligand (Figure 3). Here we used the model ligand *o*-$Me_2PC_6H_4SMe$ to economize on computational time. The energy ordering for different PS-chelated and PS-bridged isomers is unknown, and these data could be useful to individuals with an interest in using PS and related donors as ligand auxiliaries. Bidentate coordination of the PS donor by $H_2Ru_3(CO)_9(\mu_3\text{-}S)$ furnishes a chiral product with $Ru_3(\mu_3\text{-}S)$ and sulfur (MeS moiety) stereogenic centers.[17] The latter chiral center can exhibit two distinct configurations for the Me group and the sulfur lone pair relative to the cluster polyhedron, and the resulting products are epimers.[18] The presence of two hydride-bridged Ru-Ru bonds adds additional complexity and serves to increase the potential number of chelated and bridged isomers. Two different sites for PS ligand chelation exist in $H_2Ru_3(CO)_7(PS)(\mu_3\text{-}S)$: one which involves the unique ruthenium atom that is bridged by both hydrides and second by coordination of one of the two remaining ruthenium centers, each of which contains a single edge-bridging hydride. The bridging of adjacent ruthenium centers by the PS ligand can take place across a hydride-bridged or as non-hydride-bridged Ru-Ru bond via (P_{ax}, S_{ax}), (P_{eq}, S_{eq}), (P_{ax}, S_{eq}), and (P_{eq}, S_{ax}) ligand arrangements.[19]

We have examined a total of thirty isomers for $H_2Ru_3(CO)_7(PS)(\mu_3\text{-}S)$ as a function of the distribution of the PS ligand and the edge-bridging hydrides about the cluster polyhedron. The hydrides in each isomer have been confined to separate Ru-Ru bonds as found in the parent cluster. There are sixteen PS-chelated and fourteen PS-bridged isomers that are grouped as pairs of epimers in Figure 3 and whose individual energies are reported in Table S1. The depicted structures show the most stable configuration about the MeS stereocenter in each isomer.[20] The relative energies (ΔG) computed for the species **C1**-**C30** range from -0.2 kcal/mol for **C2** to slightly over 23 kcal/mol for **C30**. **C2** is confirmed as the thermodynamically favored species of the group and is consistent with the solution structure formulated as $H_2Ru_3(CO)_7(\kappa^2\text{-}P_{ax}, S_{eq})(\mu_3\text{-}S)$, the dominant product at equilibrium from the reaction of **1** and PS. We have chosen species **C1** as the point of reference (0.0 kcal/mol) for the energetic ordering of these isomers because its structure matches that of the kinetic product of substitution $H_2Ru_3(CO)_7(\kappa^2\text{-}P_{eq}, S_{eq})(\mu_3\text{-}S)$. The computed ΔG of -0.2 kcal/mol between **C1** and **C2** gives a K_{eq} value of 1.40 that closely matches the value of 1.55 found experimentally and provides strong support for use of these two species in the DFT modeling studies conducted on the ligand isomerization involving cluster **2**.

The PS ligand in $H_2Ru_3(CO)_7(PS)(\mu_3\text{-}S)$ prefers to chelate a single ruthenium center as evidenced by the six lowest energy structures (**C1**-**C6**) shown in Figure 4. The relative energies of the different species are included alongside the designated label for each species. These six structures, which bind the ruthenium center that is flanked by both hydride ligands, are more stable than the alternative chelated structures whose PS-chelated ruthenium atom supports a single edge-bridging hydride. The energy difference between **C1**-**C6** is small (<2.3 kcal/mol) and there exists a stereochemical preference for an axial Me_2P group versus the MeS group. The energy difference between the **C1**/**C3**, **C2**/**C4**, and **C5**/**C6** epimers is also small in these isomers but larger in others.

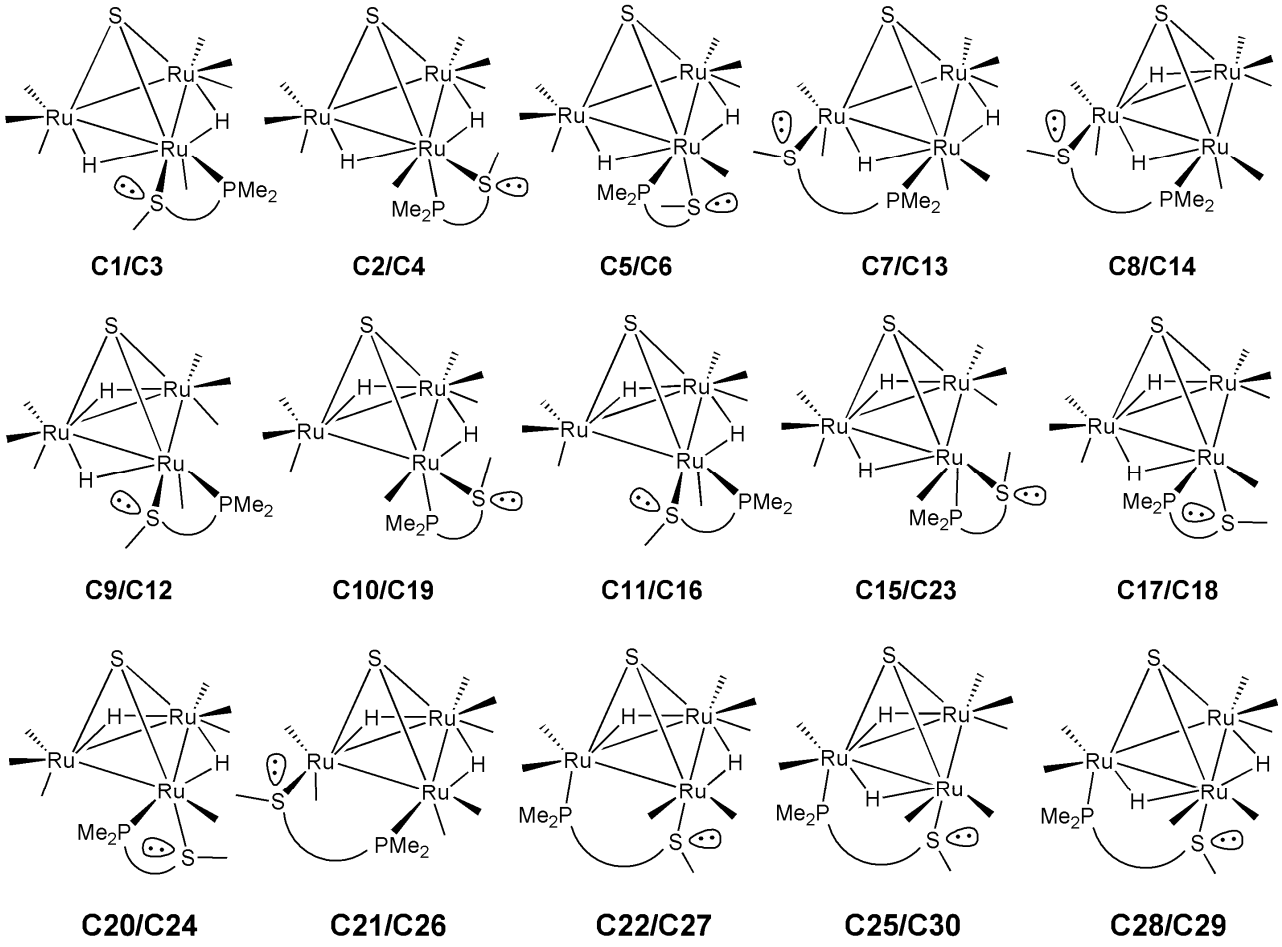

Figure 3. Computed isomers **C1**-**C30** for the chelated and bridged forms of $H_2Ru_3(CO)_7(PS)(\mu_3\text{-}S)$. The species are grouped as epimeric pairs that are related by a configurational change of the MeS moiety with the first label representing the more stable epimer.

The lowest energy PS-bridged clusters correspond to the epimeric pairs **C7**/**C8** and **C13**/**C14** and the bridged isomers **C21** and **C22** that lie ≥6.5 kcal/mol above **C1**. The DFT data confirm the preference for a chelated PS ligand in this particular cluster as confirmed experimentally (*vide supra*) and computationally for species **C1**-**C6**. Figure S2 shows the optimized structures of the thermodynamically favored PS-bridged clusters in $H_2Ru_3(CO)_7(PS)(\mu_3\text{-}S)$. A few trends exist that are worth noting in terms of the ligand distribution in these bridged species. The coordination of the PS ligand at the adjacent equatorial sites in **C7** is favored by 7 kcal/mol over the corresponding axial orientation displayed by the PS ligand in **C22**. For those isomers with an equatorial PS ligand, a regiochemical preference exists for the coordination of the PMe_2 group by the ruthenium center that supports both bridging hydrides with **C7** and **C13** being more stable than their MeS counterparts **C8** and **C14**, respectively. Within each pair of PS-bridged epimers, the stereoisomer whose sulfur-bound Me group is proximally situated to the axial Me group of the PMe_2 moiety is sterically destabilized relative to the epimer with a distal Me-S moiety. The energy difference (ΔG) between the epimers **C7**/**C13** and **C8**/**C14** is comparable in magnitude (ca. 3.7 kcal/mol). Finally, the least stable isomers in this family involve an axially disposed PS ligand that shares a Ru-Ru bond with an edge-bridged hydride. The ancillary hydrides in all of the computed species lie below the metallic plane and opposite the capping sulfido group. The locus adopted by such a hydride places it unfavorably close to the axially bridged PS ligand and within the van der Waals contact with the syn equatorial CO group at each ruthenium center that is tethered by the two bridging groups.

III. Computational Study on the Formation of $H_2Ru_3(CO)_7(\kappa^2\text{-}P_{eq}, S_{eq})(\mu_3\text{-}S)$ (C1) from Cluster 1 and PS. The formation of the kinetic substitution product **C1** from cluster **1** and PS donor was investigated by electronic structure calculations. The transformation of **1** (**A**) + PS (**B**) → **C1** proceeds by a sequence of eleven steps, and Figure 5 shows the participating clusters en route to **C1**.

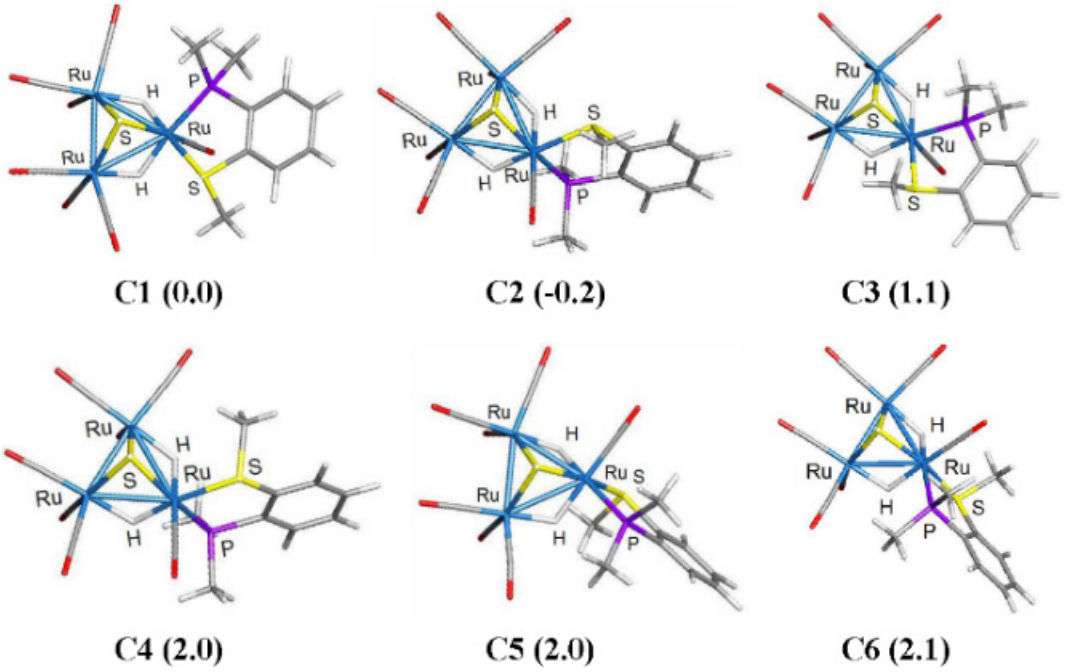

Figure 4. Optimized structures for selected chelated isomers with the energy values (ΔG in kcal/mol) contained in the parentheses and referenced to species **C1**.

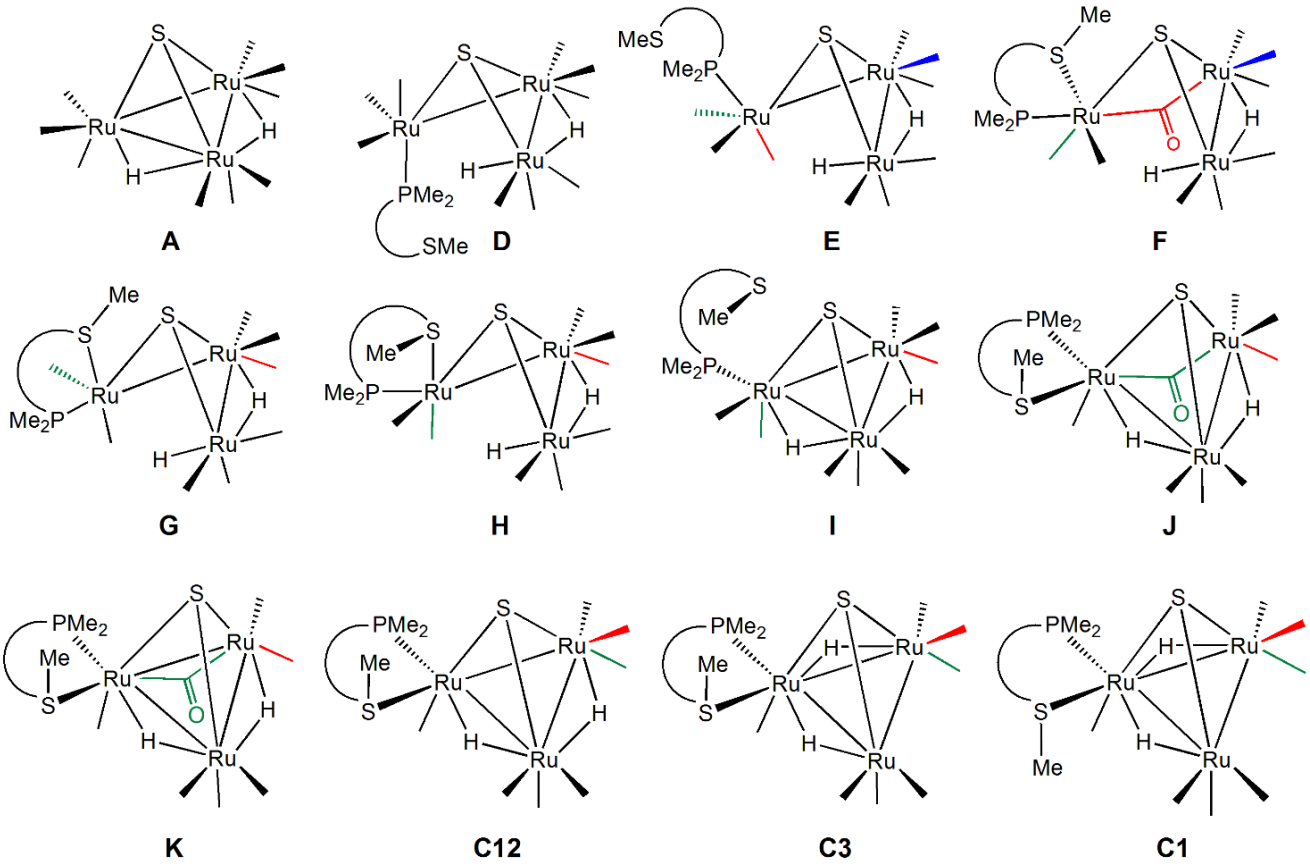

Figure 5 Bond-line structures for the Ru_3 participants in the conversion of cluster **1** (**A**) to $H_2Ru_3(CO)_7(\kappa^2\text{-}P_{eq}, S_{eq})(\mu_3\text{-}S)$ (**C1**). The structures for the PS donor (**B**) and the liberated CO are not shown.

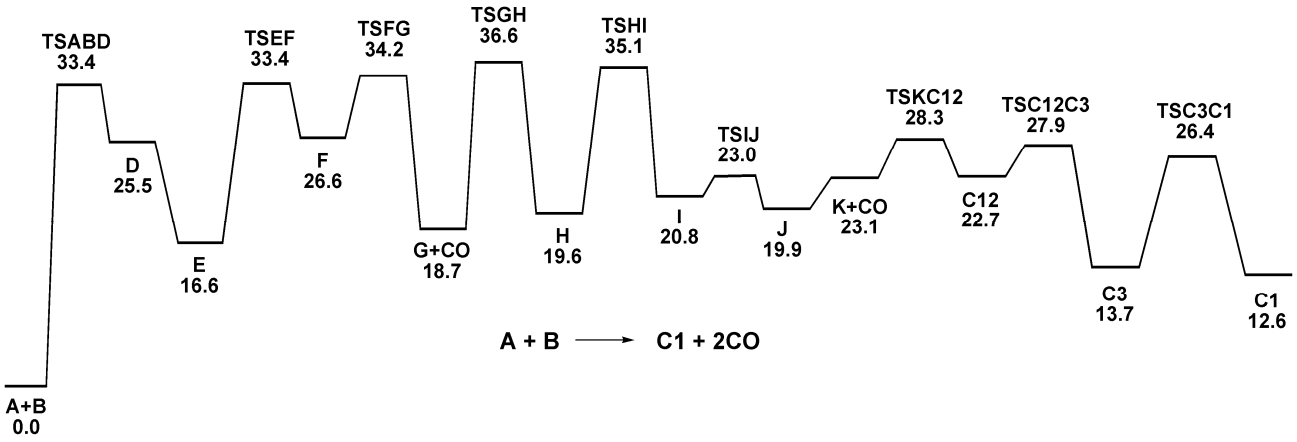

Figure 6. Free-energy profile for the conversion of **A** + **B** → **C1** + 2CO. Energy values are ΔG in kcal/mol with respect to **A** and **B**.

The addition of the PS donor (species **B**) to cluster **1** (species **A**) exhibits twofold regiospecificity that involves the exclusive addition of the phosphine moiety of **B** to one of the monohydride-bridged ruthenium centers in **A**. Phosphine addition to **A** occurs below the metallic plane trans to the capping sulfido ligand. The formation of the P-Ru bond (κ^1-PS) is accompanied by the polyhedral expansion of the adjacent hydride-bridged Ru-Ru bond to yield to the opened cluster **D** in a process that underscores the coordinative flexibility in metal clusters where metal-metal and metal-ligand vertex bonds serve as latent coordination sites for ligand addition and substrate activation reactions.[21-23] **D** lies 25.5 kcal/mol above the reactants (Figure 6) and is tangentially related to the expanded clusters found by Planalp and Vahrenkamp in the ligand-induced openings of the phosphinidene-capped tetrahedral clusters $FeCo_2(CO)_9(\mu_3$-PMe) and $FeCoWCp'(CO)_8(\mu_3$-PMe) (where Cp' = Cp, Cp*).[24,25] In that study, several PMe_3- and $PPhMe_2$-substituted products were characterized by spectroscopic and crystallographic methods, and phosphine addition (two equivs) was shown to occur with the scission of two metal-metal bonds through an associative addition process. Scheme 4 illustrates the sequence for the $FeCo_2$ cluster. No evidence for ligand slippage of the phosphinidene vertex ($\mu_3 \rightarrow \mu_2$) was observed in these reactions, but such an intermediate could have escaped detection if it were short-lived.

Scheme 4. Cluster opening in $FeCo_2(CO)_9(\mu_3$-PMe) by PMe_3 addition.

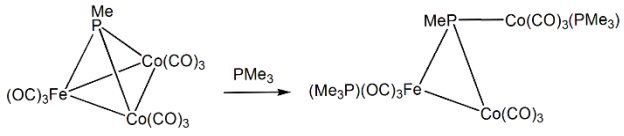

Our data represent the first computational study, to our knowledge, that documents the ligand-induced opening of a hydride-bridged metal-metal bond in a tetrahedral cluster. Ligand-induced scission of unsupported metal-metal bonds and metal-capping ligand bonds is known, but the conversion of a hydride-bridged Ru-Ru bond to a terminal hydride group in a metal cluster following ligand addition is unprecedented. Hydride mobility in metal clusters is well-documented, and fluxionality involving hydride transit across intact metal-metal bonds via bridge-terminal-bridge exchange sequences while common,[26] does not result in the formation of a terminal metal-hydride (M-H) at the expense of the original metal-metal bond.

Figure 7 shows the optimized ground-state structures for the reaction leading to **C1**. Isomerization of **D** → **E** follows the formation of the addition adduct, and this furnishes the more stable rotational isomer that lies 8.9 kcal/mol lower in energy. The total electron count and the six-coordinate environment at the P-substituted ruthenium atom remain unchanged in this transformation. The formation of **E** is driven by the unfavorable van der Waals interactions that exist between the Ru-H ligand and the methyl groups of the Me_2P ligand in **D**. These close contacts are eliminated on the isomerization of the PS ligand to the exo site in **E**. The Ru-Ru bond in **E** is over 4.00 Å in length and this distance precludes any bonding interaction between the P-substituted ruthenium center and the adjacent Ru-H centers in **E**.[27,28]

The chelation of the pendant MeS moiety in **E** occurs next, and the coordination of the sulfur donor is coupled with the synchronous migration of the axial CO (red, trans to the phosphine) to the adjacent ruthenium center to give **F**. The formation of a bridging CO (red) group at the expense of the old Ru-Ru bond allows the Ru(κ^2-PS) center to maintain an octahedral geometry. Transit of the bridging CO (red) to the

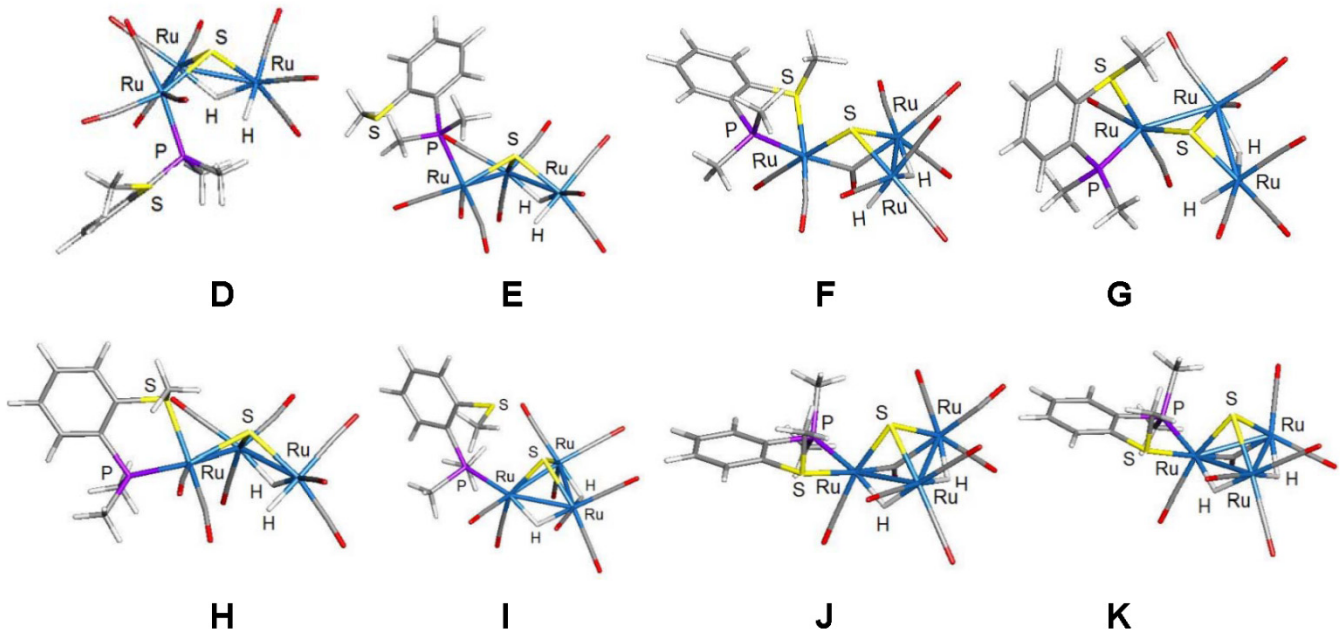

Figure 7. Optimized structures for the intermediates **D**-**K**.

adjacent ruthenium gives **G** whose formation is accompanied by the release of the equatorial CO (blue) and regeneration of the original Ru-Ru bond. The κ^2-PS ligand in **G** exhibits a P_{eq}, S_{ax} disposition with the P donor situated pseudo trans to the Ru-Ru bond based on the P-Ru-Ru bond angle of ca. 147°, while the MeS moiety lies above the metallic plane capped by the μ_3-sulfido group. Tripodal rotation of the PMe_2 and CO groups at the PS-chelated ruthenium center reorients and places the larger PMe_2 group at a less crowded equatorial site in **H**.[29] The $Ru_3(\mu_3$-S) tetrahedron is regenerated upon bond-pair donation from the terminal Ru-H moiety to the PS-substituted ruthenium center which occurs with the release of the coordinated MeS group to give **I**. This latter species likely serves as the precursor to the resting state isomer observed by NMR spectroscopy.[30]

The three ligands at the PS-substituted ruthenium in **I** are properly aligned with respect to the non-hydride-bridged Ru-Ru bond to support the conrotation of the two CO groups that is triggered by the chelation of the MeS moiety. Here the migration of the axial CO (green) to the adjacent ruthenium center is promoted by the addition of the MeS moiety to the ruthenium center and this affords **J** in a process reminiscent of that described for the formation of **F**. Dissociative loss of the CO in **J** furnishes **K** which still maintains the original bridging CO (green) moiety. The in-plane migration of the CO (green) group to the axial site at the adjacent ruthenium completes the process and gives the PS-chelated product **C12**, whose structure was addressed earlier in our study on the stability of the different isomers based on $H_2Ru_3(CO)_7(PS)(\mu_3$-S).

While **C12** possesses the same molecular formula as the kinetic substitution product **C1**, the locus of one hydride and the Me/lone pair disposition at the stereogenic MeS center are both wrong, making this isomer 10.1 kcal/mol less stable than **C1**. Migration of the remote hydride to the metallic edge cis to the PMe_2 group furnishes **C3**, which in turn epimerizes via a pyramidalization[17b,31] that involves **TSC3C1** with a forward barrier height of 12.7 kcal/mol to complete the sequence and give the kinetic product **C1**.

IV. Kinetic modeling of the PS ligand isomerization in $H_2Ru_3(CO)_7(\kappa^2$-PS)(μ_3-S): Conversion of 2-(P_{eq}, S_{eq}) → 2-(P_{ax}, S_{eq}). The isomerization reaction was investigated kinetically by following the evolution of **2**-(P_{eq}, S_{eq}) and **2**-(P_{ax}, S_{eq}) to equilibrium over the temperature range 298-323 K, and the data were successfully fit to a model based on a reversible first-order reaction involving **2**-(P_{eq}, S_{eq}) ⇌ **2**-(P_{ax}, S_{eq}).[32,33] The rate to equilibrium is best measured by starting with **2**-(P_{eq}, S_{eq}) at a point of maximum displacement from equilibrium. The reaction of **1** with PS in the presence of Me_3NO reliably furnished an 85:15 mixture of **2**-(P_{eq}, S_{eq}) and **2**-(P_{ax}, S_{eq}). The boundary conditions employed in our modeling studies reflect the initial ratio of the two products. The course of the isomerization was conveniently monitored by either ^{1}H NMR spectroscopy or HPLC. Figure S3 shows the NMR spectral changes as a function of time for the reaction investigated at 303.0 K. These data were successfully modeled, and the ^{1}H NMR data for the conversion versus time profiles for **2**-(P_{eq}, S_{eq}) and **2**-(P_{ax}, S_{eq}) are depicted in Figure 8. Excellent agreement is confirmed for the nonlinear regression treatment of the data according to the reversible first-order equilibrium (Eq 1).

$$\mathbf{2}\text{-}(P_{eq},S_{eq}) \underset{k_2}{\overset{k_1}{\rightleftharpoons}} \mathbf{2}\text{-}(P_{ax},S_{eq}) \qquad (1)$$

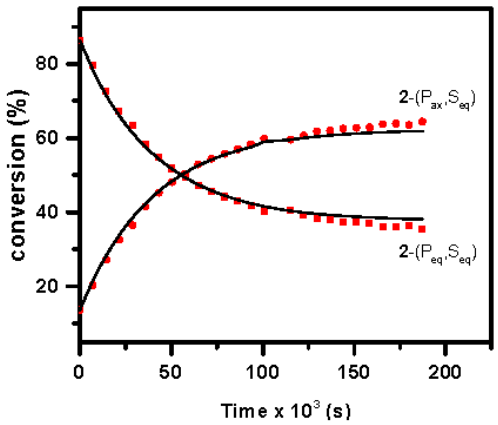

Figure 8. ^{1}H NMR measured conversion (•) versus time profile for the isomerization of **2**-(P_{eq}, S_{eq}) ⇌ **2**-(P_{ax}, S_{eq}) at 303.0 K. The solid lines represent the non-linear regression fit for a reversible first-order reaction.

The forward (k_1) and reverse (k_2) rate constants for the isomerization are reported in Table 1, along with the equilibrium constant as a function of temperature. Figure S4 shows the plots of ln(k/T) versus T^{-1} from which the Eyring activation parameters were computed for the forward [$\Delta H^{\ddagger}$ = 21.2(6) kcal/mol and $\Delta S^{\ddagger}$ = -10(2) eu] and the reverse [$\Delta H^{\ddagger}$ = 19.5(7) kcal/mol and $\Delta S^{\ddagger}$ = -17(2) eu] steps. Both reaction steps exhibit a negative $\Delta S^{\ddagger}$ value that is consistent with an ordered transition state for the tripodal rotation.

Table 1. Forward (k_1) and Reverse (k_2) Rate Constants and Equilibrium Constants (K_{eq}) for the Isomerization of 2-(P_{eq},S_{eq}) ⇌ 2-(P_{ax},S_{eq})

Temp (K)	k_1	k_2	K_{eq}[c]
293.0	4.60(34)e-6	3.17(11)e-6	1.45(4)
298.0[b]	7.41(47)e-6	4.78(13)e-6	1.55(5)
303.0	1.54(5)e-5	9.30(20)e-6	1.66(5)
303.0[b]	1.11(12)e-5	6.76(30)e-6	1.65(5)
313.0	4.70(3)e-5	2.71(1)e-5	1.73(5)
323.0	1.35(1)e-4	6.98(3)e-5	1.91(6)

[a]Rate constants are in s^{-1} and are from ^{1}H NMR measurements unless otherwise noted. [b]HPLC collected data. [c]Ratio of **2**-(P_{ax},S_{eq})/**2**-(P_{eq},S_{eq}).

The van't Hoff plot for the isomerization is depicted in Figure S5. The computed values for ΔH [1.69(7) kcal/mol] and ΔS [6.5(2) eu] reveal that the isomerization, while enthalpically unfavorable, is entropically driven to product above 262 K. This suggests that the cluster is better able to accommodate the ancillary ligands in the product [**2**-(P_{ax}, S_{eq})] relative to the kinetically formed product that has a slightly more restricted ligand sphere based on a P_{eq}, S_{eq} ligand orientation.

V. Computational Study on the Isomerization of C1 ⇌ C2. With the mechanism for the formation of **C1** (kinetic isomer) mapped out and the isomerization between the chelated products of **2** kinetically modeled, we now address the isomerization mechanism for **2**-(P_{eq}, S_{eq}) ⇌ **2**-(P_{ax}, S_{eq}). We investigated several reaction paths by DFT and were able to rule out a dissociative manifold involving the release of either the Me_2P or MeS moiety to furnish an unsaturated intermediate with the general formula $H_2Ru_3(CO)_7(\kappa^1$-PS). The transition-state energies for these alternative intermediates lie >12 kcal/mol above the rate-limiting barrier in the preferred mechanism whose details are discussed in the next section.

The concerted tripodal rotation of the three ligands at the Ru(CO)(κ^2-PS) center was next investigated because it would allow **C1** to transform directly to **C2** and fulfill the kinetic modeling based on a reversible first-order process. Figures 9 and 10 show the energy profile and the optimized structures for two of the isomerization reactions we will discuss in detail. Starting with **C1** (Figure 4), a clockwise rotation of the three rotor ligands at Ru(CO)(κ^2-PS) affords **TSC1C2** with a barrier of 29.1 kcal/mol. This rotation leads to three eclipsing interactions in **TSC1C2**, two of which involve a bridging hydride that is proximally situated to the CO and Me_2P rotor groups, with the third eclipsing interaction involving the MeS and capping sulfido groups. All three interactions are well within the van der Waals radii of the H/CO, H/PMe_2, and S/SMe groups and serve as significant contributors to the overall barrier.

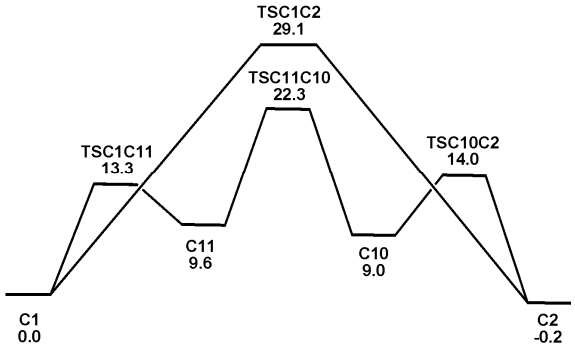

Figure 9. Potential energy profile for the isomerization of **C1** ⇌ **C2**. Energy values are ΔG in kcal/mol with respect to **C1**.

The computed barrier for **TSC1C2**, while not unreasonable, lies 4.9 kcal/mol above the $\Delta G^{\ddagger}$ measured in the kinetics experiments for the forward step of the isomerization reaction. Accordingly, we examined the effect of hydride migration as a prerequisite step in the conversion of **C1** ⇌ **C2** due to the reported exchange broadening of the bridging hydrides in related Ru_3 and Os_3 systems.[5,6,15,16] Migration of the hydride syn to the

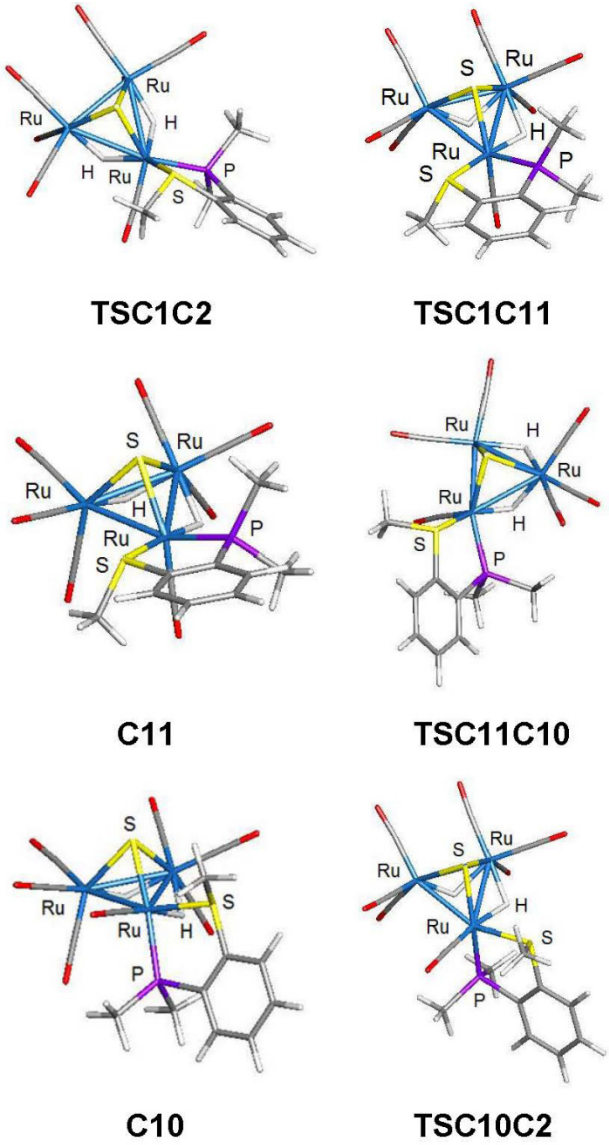

Figure 10. Optimized structures for the intermediates **C10** and **C11**, and transition-state structures **TSC1C2**, **TSC1C11**, **TSC11C10**, and **TSC10C2**

MeS moiety in **C1** to the adjacent non-hydride bridged Ru-Ru bond proceeds by **TSC1C11** and yields the hydride isomer **C11**. Hydride transit occurs across the polyhedral face of the cluster opposite the capping sulfido moiety. Clockwise tripodal rotation of the three ligands at the Ru(CO)(κ^2-PS) center follows through **TSC11C10** whose barrier is more closely aligned with the experimental value of 24.2 kcal/mol (forward step). **TSC11C10** lies 6.8 kcal/mol lower in energy than **TSC1C2**, and the principal origin for the energy difference between the DFT-computed transition states ($\Delta\Delta G^{\ddagger}$) is attributed to the initial hydride migration in **C1** to **C11**. The latter isomer, while less stable, provides an increased measure of freedom for the subsequent tripodal rotation by eliminating the eclipsing interaction extant between the bridging hydride and the migrating CO in **TSC1C2**. Progressing from **TSC11C10** affords **C10** whose κ^2-PS ligand has the proper P_{ax}, S_{eq} orientation as that displayed in thermodynamic product **C2**, which, in turn, is produced by a final migration of the original hydride (**TSC10C2**) back to its initial locus and now syn to the axial Me_2P group in **C2**.[34] This particular sequence is illustrated in Figure S6.

We wish to point out that the multistep mechanism depicted in Figure 9 vis-à-vis the kinetic modeling data presented for the **2**-(P_{eq}, S_{eq}) ⇌ **2**-(P_{ax}, S_{eq})/(**C1** ⇌ **C2**) isomerization will exhibit reversible first-order kinetics within the steady-state approximation given the extremely low concentrations predicted for the intermediates **C11** and **C10**. The amount of these intermediates relative to **C1** and **C2** are estimated at $<10^{-6}$ based on the Boltzmann distribution of the participating ground-state species in the isomerization. Since the kinetics alone provide no insight into the existence/nature of these intermediates, we must rely on the DFT data to provide added insight for a more accurate picture on the identity of such intermediates and their energies relative to the phenomenologically observed components in this equilibrium.

The final isomerization mechanism evaluated by us is depicted in Figure 11. Here we evaluated the kinetic lability of the epimer produced from **C1** on pyramidalization of the MeS group and its participation in the isomerization. The pyramidalization of the MeS group in **C1** to give epimer **C3** proceeds via **TSC1C2** with a relatively low barrier of 13.8 kcal/mol. Tripodal rotation of the CO/PS ligands follows and transition state **TSC3C4** lies 30.4 kcal/mol above **C1**, making this the slowest step of the three processes computed for tripodal rotation. The resulting product **C4** transforms into **C2** through one last low-energy pyramidalization. While **TSC3C4** is not the preferred isomerization pathway, the data do support non-dissociative epimerization as energetically competitive paths for ligand epimerization (rearrangement) in this family of metal clusters.

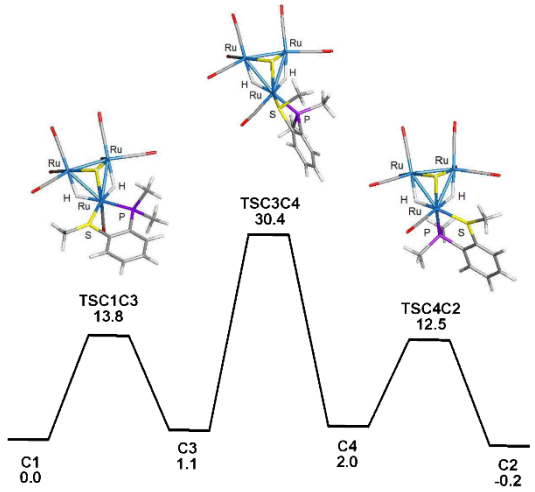

Figure 11. Potential energy profile for the isomerization of **C1** ⇌ **C2** initiated by MeS epimerization and optimized transition-state structures **TSC1C3**, **TSC3C4**, and **TSC4C2**. Energy values are ΔG in kcal/mol with respect to **C1**.

Conclusions

The reaction of 2-(diphenylphosphino)thioanisole (PS) with $H_2Ru_3(CO)_9(\mu_3\text{-}S)$ (**1**) has been investigated and found to give the chelated cluster $H_2Ru_3(CO)_7(\kappa^2\text{-}PS)(\mu_3\text{-}S)$ (**2**) in high yield, making this the first reported example of a cluster based on **1** with an ancillary PS ligand. The formation of **2** is kinetically controlled, and the chelated PS ligand is shown to occupy equatorial sites (P_{eq}, S_{eq}) in the kinetic isomer, which is unstable and rearranges to the thermodynamically more stable diastereomer where the PS ligand is bound at the axial and equatorial sites (P_{ax}, S_{eq}). The fluxional exchange between these diastereomers occurs via a tripodal rotation of the three ligands at the PS-chelated $Ru(CO)(\kappa^2\text{-}PS)$ center. The kinetics to equilibrium have been measured by NMR and HPLC methods, and the concentration versus time profiles of the diastereomers have been successfully reproduced using a kinetic model based on reversible first-order equilibrium.

The results of DFT calculations indicate that the addition of the PS donor to **1** proceeds in a regiospecific fashion via an endo addition of the phosphine to a ruthenium center that is bridged by a single hydride ligand. The ligand addition step is accompanied by an expansion of the cluster polyhedron which proceeds at the expense of a hydride-bridged Ru-Ru bond. Chelation of the MeS moiety proceeds via CO loss and ultimately affords the kinetic diastereomer. The reversible isomerization involving **2**-(P_{eq}, S_{eq}) ⇌ **2**-(P_{ax}, S_{eq}) has been evaluated computationally and shown to proceed by an initial transfer of one the bridging hydrides to the non-hydride bridged Ru-Ru bond, freeing up the environment at the $Ru(CO)(\kappa^2\text{-}PS)$ site for the ensuing tripodal rotation. Return of the hydride to the original Ru-Ru vector completes the process and furnishes the diastereomer with a P_{ax}, S_{eq} disposition.

Experimental Section

General procedures. The $RuCl_3 \cdot xH_2O$, which was used in the synthesis of $Ru_3(CO)_{12}$,[35] was purchased from Pressure Chemical Co. and used as received. The starting cluster $H_2Ru_3(CO)_9(\mu_3\text{-}S)$ was prepared from $Ru_3(CO)_{12}$ and H_2S (Specialty Gases of America Inc.) according to the published procedure.[36] The chemicals 2-bromothioanisole, Ph_2PCl, and $Me_3NO \cdot xH_2O$ were purchased from Aldrich Chemical Co., and the latter was dehydrated by azeotropic distillation from benzene. The 2-(diphenylphosphino)thioanisole (PS) employed as a ligand in this study was prepared by the procedure outlined by Reinius et al.[37] The reaction solvents used in the synthetic portion of this work were obtained from an Innovative Technology (IT) solvent purification system. HPLC grade acetonitrile and water were purchased from Fisher Chemical and J.T.Baker, respectively, and used as received. The deuterated NMR solvents CD_3CN, $CDCl_3$, and CD_2Cl_2 were purchased from Cambridge Isotope Laboratories, Inc. and dried over an appropriate drying agent before use. All synthetic reactions were conducted under argon employing standard Schlenk-line techniques. The combustion analysis was performed by Atlantic Microlab, Norcross, GA.

The ^1H NMR spectroscopic data were recorded on Varian VXR-400 or VXR-500 spectrometers at 400 MHz or 500 MHz, respectively, while the $^{31}P\{^1H\}$ NMR spectroscopic data were recorded at 161 MHz or 202 MHz on the aforementioned spectrometers, respectively. The routine NMR spectra were recorded at room temperature. The HPLC separations were performed using a Shimadzu LC-20AT preparative liquid chromatograph equipped with a Shimadzu FRC-10A fraction collector and a Premier C_{18} column with a 5µ particle size and 250 x 10 mm dimensions. All IR spectra were recorded on a Nicolet 6700 FT-IR spectrometer in amalgamated NaCl cells with a 0.1 mm path length.

Preparation of $H_2Ru_3(CO)_7(\kappa^2\text{-}P_{eq}, S_{eq})(\mu_3\text{-}S)$ and $H_2Ru_3(CO)_7(\kappa^2\text{-}P_{ax}, S_{eq})(\mu_3\text{-}S)$. To a room temperature solution of $H_2Ru_3(CO)_9(\mu_3\text{-}S)$ (50 mg, 0.085 mmol) in 25 mL of dichloromethane under argon was added Me_3NO (14 mg, 0.19 mmol). The solution was stirred for 2 mins, after which PS (26 mg, 0.085 mmol) was added, and the solution was stirred for an additional 1 h. The solvent was then removed under vacuum and analyzed by TLC, which revealed the presence of a single spot for the isomeric products (R_f = 0.43; 1:1 dichloromethane/hexanes). The products were purified by column chromatography over silica gel using a 1:1 mixture of dichloromethane/hexanes as the mobile phase. The isomeric products were eluted from the column as one fraction as a red solid in 94% yield. The isomers consisting of $H_2Ru_3(CO)_7(\kappa^2\text{-}P_{eq}, S_{eq})(\mu_3\text{-}S)$ and $H_2Ru_3(CO)_7(\kappa^2\text{-}P_{ax}, S_{eq})(\mu_3\text{-}S)$ were subsequently separated by preparative HPLC at 35 °C using an eluent composed of an 9:1 mixture of acetonitrile/water at a flow rate of 2 mL/min. The kinetic product of substitution $[H_2Ru_3(CO)_7(\kappa^2\text{-}P_{eq},S_{eq})(\mu_3\text{-}S)]$ eluted first and this was immediately followed by the thermodynamic isomer $[H_2Ru_3(CO)_7(\kappa^2\text{-}P_{ax},S_{eq})(\mu_3\text{-}S)]$. The initial ratio of the separated isomers was ca. 9:1 in favor of the faster isomer. The slower moving product was confirmed as the thermodynamically favored species. The concentration of the separated products changed accordingly over time as each diastereomer eventually reached equilibrium. IR (CH_2Cl_2, initial isomeric mixture): ν(CO) 1994 (br), 2039 (s), 2071 (s) cm^{-1}. $H_2Ru_3(CO)_7(\kappa^2\text{-}P_{eq}, S_{eq})(\mu_3\text{-}S)$ (kinetic product): ^1H NMR (500 MHz, $CDCl_3$): δ -20.11 (1H, broad dd, $^2J_{HP}$ 9.54, $^2J_{HH}$ 1.79 Hz, hydride), -17.26 (1H, dd, $^2J_{HP}$ 34.00, $^2J_{HH}$ 1.79 Hz, hydride), 2.75 (3H, s, SCH3), 7.30-7.65 (13H, m, aryl), 7.85 (1H, dd, J_{HH} 7.75, 1.79 Hz, aryl). ^{31}P NMR (202 MHz, $CDCl_3$): δ 67.46. $H_2Ru_3(CO)_7(\kappa^2\text{-}P_{ax}, S_{eq})(\mu_3\text{-}S)$ (thermodynamic product): ^1H NMR (500 MHz, $CDCl_3$): δ -18.94 (1H, dd, $^2J_{HP}$ 8.34, $^2J_{HH}$ 2.38 Hz, hydride), -18.78 (1H, dd, $^2J_{HP}$ 11.33, $^2J_{HH}$ 2.38 Hz, hydride), 2.80 (3H, s, SCH3), 7.30-7.60 (13H, m, aryl), 7.82 (1H, dd, J_{HH} 8.34, 1.79 Hz, aryl). ^{31}P NMR (202 MHz, $CDCl_3$): δ 65.91. Anal. Calcd (found) for $C_{26}H_{19}O_7PRu_3S \cdot ½$benzene: C, 39.51 (39.93); H, 2.50 (2.89).

X-ray Crystallography. Single crystals of $H_2Ru_3(CO)_7(\kappa^2\text{-}P_{eq}, S_{eq})(\mu_3\text{-}S)$ suitable for X-ray diffraction analysis were grown from an equilibrium mixture of cluster **2** dissolved in CH_2Cl_2 that was layered with heptane. X-ray quality crystals of $[H_2Ru_3(CO)_8(\mu_4\text{-}S)]_3 \cdot CH_2Cl_2$ were grown similarly from a CH_2Cl_2 solution containing the trimer that was layered with heptane. Both crystallizations were conducted at 0 °C under argon.

The X-ray data for $H_2Ru_3(CO)_7(\kappa^2\text{-}P_{eq}, S_{eq})(\mu_3\text{-}S)$ and $[H_2Ru_3(CO)_8(\mu_4\text{-}S)]_3 \cdot CH_2Cl_2$ were collected using a Rigaku

XtaLAB Synergy-S diffractometer equipped with a HyPix-6000HE Hybrid Photon Counting (HPC) detector and dual Mo and Cu microfocus sealed X-ray source. Both datasets were collected at 100(2) K using a low-temperature Oxford Cryostream 800 liquid nitrogen cooling system. The data were collected and processed using the commercial program CrysAlisPro (1.171.40.12b; Rigaku Oxford Diffraction, 2018) to ensure desired data redundancy and percent completeness. Absorption correction was performed using the SCALE3 ABSPACK scaling algorithm present in the CrysAlisPro software. The structures were solved using ShelXT,[38] and all non-hydrogen atoms were refined anisotropically using ShelXL.[39] The space group for each structure was unambiguously verified by PLATON.[40] Bridging hydrogen atoms in both compounds were localized in the difference Fourier map and refined freely with an isotropic displacement parameter. The remaining hydrogen atoms in both structures were attached via the riding model at calculated positions. Olex24[41] was used for the preparation of the different materials reported in this publication.

Computational Methodology. All DFT calculations were carried out with the Gaussian 09 suite of programs[42] using TPSS as the functional with auto density fitting sets enabled.[43] Our choice of this particular functional was dictated by the accurate calculation of the ground-state energy difference between the isomeric cluster $H_2Ru_3(CO)_7(\kappa^2\text{-PS})(\mu_3\text{-S})$ products. Several different functionals were initially screened and found to give grossly incorrect product energies that favored the kinetic isomer over the thermodynamic isomer. The ruthenium atoms were described with a Stuttgart-Dresden effective core potential and SDD basis set,[44] while the 6-31G(d') basis set[45] was employed for the remaining atoms.

To facilitate the computations the phenyl groups of the PS ligand were replaced with methyl groups. All reported geometries were fully optimized with no restraints, and the analytical second derivatives were evaluated at each stationary point and verified as an energy minimum (positive eigenvalues) or a transition structure (one negative eigenvalue). The enthalpic and entropic corrections were made from the unscaled vibrational frequencies, and the resulting free energies are reported in kcal/mol relative to the specified standard. Standard state corrections were applied to all species to convert concentrations from 1 atm to 1 M following the treatment outlined by Cramer.[46] Intrinsic reaction coordinate (IRC) calculations were performed on all transition states to establish the reactant and product species associated with the different transition-state structures. The geometry-optimized structures reported here were reproduced with the JIMP2 molecular visualization and manipulation program.[47]

Isomerization Kinetics. The kinetics to equilibrium for **2**-(P_{eq},S_{eq}) ⇌ **2**-(P_{ax},S_{eq}) were investigated by ^{1}H NMR spectroscopy and HPLC over the temperature range 293-323 K, with the former studies carried out in $CDCl_3$ solvent in NMR tubes equipped with a J-Young valve that allowed the sample to be freeze-pump-thaw-degassed prior to active measurement. The NMR experiments were conducted in the NMR probe, and the progress of the reaction was followed as a function of the intensity of the hydride resonances until the ratio of the two isomers reached equilibrium. Clean interconversion between the isomers was confirmed under these conditions, and no observable decomposition was found over the course of the reaction. The reported temperature is assumed to be accurate to within ±0.5 K. The HPLC kinetics were performed in CH_2Cl_2 solvent, and the samples were sealed in a Schlenk tube under argon. The reaction vessel contained a screw-top Teflon cap, allowing aliquots to be withdrawn by syringe as needed. The temperature of the samples was maintained by a Thermo-Scientific NESLAB RTE7 circulating bath with an accuracy of ±0.5 K. The reaction was sampled as a function of time and the aliquots were analyzed by HPLC, and the relative concentration of each isomer was determined from the area associated with each peak. The integration procedure employed the peak fitting software available with the HPLC instrument, and the peak integrals were obtained by fitting the experimental data with a Gaussian function. The individual rate constants (k_1 and k_2) to equilibrium were extracted from k_{eq} by nonlinear regression analysis using the below expressions (Eqs 2 and 3) that were derived from the reaction of **2**-(P_{eq}, S_{eq}) (**A**) ⇌ **2**-(P_{ax}, S_{eq}) (**B**) (Eq 1). The rate constants (k_1 and k_2) were treated as free variables in the regression analysis that minimized the sum of the squares of the residuals for the amount of each species as a function of time. The activation parameters for the approach to equilibrium for each species were calculated from the plots of ln(k/T) versus T^{-1} while the parameters ΔH and ΔS values at equilibrium were obtained from a van't Hoff plot of ln(K_{eq}) versus T^{-1}.[48]

$$A_t = A_0 e^{-(k_1+k_2)t} + \left(\frac{k_2}{k_1+k_2}\right)(A_0+B_0)\left[1-e^{-(k_1+k_2)t}\right] \quad (2)$$

$$B_t = B_0 e^{-(k_1+k_2)t} + \left(\frac{k_1}{k_1+k_2}\right)(A_0+B_0)\left[1-e^{-(k_1+k_2)t}\right] \quad (3)$$

ASSOCIATED CONTENT

Supporting Information.
The Supporting Information is available free of charge on the ACS Publications website at DOI: xxxxxxxxx. Crystallographic data, atomic coordinates and energies for all DFT-reported species, selected DFT-optimized structures and kinetic fits of the isomerization of cluster **2** to equilibrium, and derivation of the integrated rate expression for a reversible first-order equilibrium that was used in the kinetic modeling reported here.

Accession Codes
CCDC 1891991 and 189992 contain the supplementary crystallographic data for this paper. These data can be obtained free of charge via www.ccdc.cam.ac.uk/data_request/cif, or by emailing data_request@ccdc.cam.ac.uk, or by contacting The Cambridge Crystallographic Data Centre, 12 Union Road, Cambridge CB2 1EZ, UK; fax: +44 1223 336033.

Corresponding Author

*E-mail: cobalt@unt.edu

ORCID

Michael G. Richmond: 0000-0001-6641-866X

Author Contributions

The manuscript was written with contributions from all authors: DDM (experimental, computational, and manuscript preparation); VNN (X-ray structures); and MGR (advisor and global oversight).

Notes

The authors have no competing financial interests to declare.

ACKNOWLEDGMENT

We wish to thank Profs. Paul Marshall and Joseph Iaia for helpful comments on modeling reversible first-order reactions. Financial support from the Robert A. Welch Foundation (Grant B-1093-MGR) is acknowledged, as is the NSF for the purchase of a computer cluster and X-ray Diffractometer (CHE-1531468 and CHE-1726652).

ABBREVIATIONS

PS, 2-(diphenylphosphino)thioanisole; NMR, Nuclear Magnetic Resonance; HPLC, High-Performance Liquid Chromatography; DFT, Density Functional Theory.

REFERENCES

(1) Persson, R.; Monari, M.; Gobetto, R.; Russo, A.; Aime, S.; Calhorda, M.-J.; Nordlander, E. Synthesis and Characterization of Triosmium Clusters Containing the Bidentate Ligand $Ph_2PCH_2CH_2SMe$: Detection of an Isomerization Reaction Involving Bridging and Chelating Ligand Coordination Modes. *Organometallics* **2001**, *20*, 4150.

(2) Hrovat, D. A.; Nordlander, E.; Richmond, M. G. Investigation of the Mechanism of Phosphine-Thioether Isomerization in the Triosmium Cluster $Os_3(CO)_{10}(Ph_2PCH_2CH_2SMe)$: Migratory Preference for the Formation of an Edge-Bridged Thioether versus a Phosphine Moiety. *Organometallics*, **2012**, *31*, 6608.

(3) (a) Persson, R.; Stchedroff, M. J.; Uebersezig, B.; Gobetto, R.; Steed, J. W.; Prince, P. D.; Monari, M.; Nordlander, E. Synthesis, Characterization, and Novel Fluxional Mechanisms of Triosmium Clusters Containing the Highly Flexible Ligand $Ph_2PC_2H_4SC_2H_4SC_2H_4PPh_2$ (PSSP). *Organometallics* **2010**, *29*, 2223. (c) Persson, R.; Stchedroff, M. J.; Gobetto, R.; Carrano, C. J.; Richmond, M. G.; Monari, M.; Nordlander, E. Synthesis, Characterization, and Dynamic Behaviour of Triosmium Clusters Containing the Tridentate Ligand $\{Ph_2PCH_2CH_2\}_2S$ (PSP). *Eur. J. Inorg. Chem.* **2013**, 2447.

(4) Abdel-Magied, A. F.; Singh, A. K.; Haukka, M.; Richmond, M. G.; Norlander, E. Diastereomeric control of enantioselectivity: evidence for metal cluster catalysis. *Chem. Commun.* **2014**, *50*, 7705.

(5) For the first report on the reaction of $H_2Ru_3(CO)_9(\mu_3\text{-}S)$ with a diphosphine to give $H_2Ru_3(CO)_7(\mu\text{-}PP)(\mu_3\text{-}S)$, see: Bruce, M. I.; Shawkataly, O. B.; Snow, M. R.; Tiekink, E. R. T. Cluster chemistry. XLIII. Sulfur-carbon bond cleavage reactions in the hydrogenation of some sulfur-containing ruthenium carbonyl cluster complexes: X-ray structure of $Ru_3(\mu\text{-}H)_2(\mu_3\text{-}S)[\mu\text{-}(Z)\text{-}Ph_2PCH{:}CHPPh_2](CO)_7$. *Aust. J. Chem.* **1986**, *39*, 1109.

(6) (a) Hyder, M. I.; Begum, N.; Sikder, M. D. H.; Hossain, G. M. G.; Hogarth, G.; Kabir, S. E.; Richard, C. J. Synthesis and structure of sulfur and selenium capped dihydride triruthenium clusters $[Ru_3(CO)_7(\mu\text{-}H)_2(\mu\text{-dppm})(\mu_3\text{-}E)]$ (E = S, Se). *J. Organomet. Chem.* **2009**, *694*, 304. (b) Sikder, M. D. H.; Ghosh, S.; Kabir, S. E.; Hogarth, G.; Tocher, D. A. Chalcogenide-capped triruthenium clusters: X-ray structures of $[Ru_3(CO)_6(\mu_3\text{-}CO)\{P(C_4H_3S)_3\}(\mu\text{-dppm})(\mu_3\text{-}O)]$ and $[(\mu\text{-}H)_2Ru_3(CO)_6\{P(C_4H_3S)_3\}(\mu\text{-dppm})(\mu_3\text{-}S)]$. *Inorg. Chim. Acta* **2011**, *376*, 170. (c) Hernández-Cruz, M. G.; Zuno-Cruz, F. J.; Alvarado-Rodríguez, J. G.; Rosales-Hoz, M. J.; Leyva, M. A.; Salazar, V.; Sánchez-Cabrera, G. Reactivity of triruthenium diphosphine clusters with 3,5-bis(trifluoromethyl)mercaptobenzene: Electronic and steric influence of diphosphines onto coordination modes of thiolate, capping sulfide, and phosphide groups to Ru_3 clusters. *J. Organomet. Chem.* **2016**, *801*, 157. (d) Fompeyrine, P.; Lavigne, G.; Bonnet, J.-J. High-yield Syntheses of Sulphido Triruthenium Carbonyl Cluster Complexes containing Bis(diphenylphosphino)methane. *Dalton Trans.* **1987**, 91.

(7) For the only other known PS-chelated cluster with bridging hydrides, see: Gracheva, E. V.; Krupenya, D. V.; Pilyugina, T. S.; Tunik, S. P.; Pursiainen, J.; Haukka, M. Reactions of carbonyl clusters with heterobidentate ligands. Synthesis and structural characterization of $H_4Ru_4(CO)_{10}[k^2(P,S)\text{-}Ph_2P(2\text{-}CH_3SC_6H_4)]$ and $Rh_6(CO)_{14}[k^2(P,S)\text{-}Ph_2P(2\text{-}CH_3SC_6H_4)]$ clusters. *Russ. J. Gen. Chem.* **2006**, *76*, 682.

(8) In keeping with traditional nomenclature for $M_3(\mu_3\text{-}X)$ tetrahedral clusters, equatorial sites refer to those ligand positions that are situated pseudo planar to the three metals and axial sites correspond to those positions that lie below the metallic plane and opposite the face-capping ligand. See: Penfold, B. R.; Robinson, B. H. Tricobalt Carbon, an Organometallic Cluster. *Acc. Chem. Res.* **1973**, *6*, 73.

(9) Adams, R. D.; Katahira, D. A. Oxidative cleavage of metal-metal bonds in heteronuclear clusters. Reaction of tin tetrachloride with $(\mu\text{-}H)_2(\mu_3\text{-}S)Ru_3(CO)_9$ and the crystal and molecular structures of $(\mu\text{-}H)_2(\mu_3\text{-}S)Ru_3(CO)_9$ and $(\mu\text{-}H)_2(\mu_3\text{-}S)(\mu\text{-}Cl)Ru_3(CO)_8(SnCl_3)$. *Organometallics* **1982**, *1*, 53.

(10) Ashby, M. T.; Alguindigue, S. S.; Schwane, J. D.; Daniel, T. A. Regular and Inverse Secondary Kinetic Enthalpy Effects (KHE) for the Rate of Inversion of Thioether and 1,1′-Biisoquinoline Complexes of Ruthenium and Osmium. *Inorg. Chem.* **2001**, *40*, 6643, and references therein.

(11) The small $^2J_{HH}$ coupling in the high-field resonance was partiaally obscured by line broadening and possibly reflects anisotropic screening that is promoted by the lone-electron pair on the thioether moiety.

(12) Hodge, S. R.; Johnson, B. F. G.; Lewis, J.; Raithby, P. R. Trinuclear Osmium Clusters containing Bidentate $Ph_2PCH_2PPh_2$ and $Me_2PCH_2PMe_2$ Ligands: X-Ray Crystal Structures of the Complexes $[Os_3H(CO)_9(Me_2PCHPMe_2)]$ and $[Os_3H(OH)(CO)_8(Ph_2PCH_2PPh_2)]$. *Dalton Trans.* **1987**, 931.

(13) Farrugia, L. J.; Freeman, M. J.; Green, M.; Orpen, A. G.; Stone, F. G. A.; Salter, I. D. Metal framework arrangements in pentanuclear gold-ruthenium clusters. Crystal structures of $[Au_2Ru_3(\mu_3\text{-}S)(CO)_8(PPh_3)_3]$ and $[Au_2Ru_3(\mu\text{-}H)(\mu_3\text{-}COMe)(CO)_9(PPh_3)_2]$. *J. Organomet. Chem.* **1983**, *249*, 273.

(14) Dyson, P. J.; McIndoe, J. S. *Transition Metal Carbonyl Cluster Chemistry*. Gordon and Breach Science Publishers, 2000; pp. 95-96.

(15) Ali, A.; Deeming, A. J.; Hogarth, G.; Mehta, N. A.; Steed, J. W. Reductive coupling of alkynes to give ruthenium and osmium clusters of the type $[M_3(1,3\text{-diene})(\mu_3\text{-}X)(CO)_8]$ containing $\mu\text{-}\eta^2,\eta^2$- or η^4-1,3-diene. *Chem. Comm.* **1999**, 2541.

(16) Adams, R. D.; Männig, D.; Segmüller, B. E. The Oligomerization of Clusters. The Synthesis and Crystal and Molecular Structure of $[(\mu\text{-}H)_2(\mu_4\text{-}S)Ru_3(CO)_8]_3$. *Organometallics* **1983**, *2*, 149.

(17) (a) The coordination of pnictogen and chalcogen donor moieties in $H_2Ru_3(CO)_7(\kappa_2\text{-}PS)(\mu_3\text{-}S)$ produces two stereogenic centers based on an asymmetric SRu_3 tetrahedron and chiral MeS moiety. Interconversion between cluster diastereomers can take place by epimerization of the Me group and lone electron pair associated with the MeS moiety through either a MeS dissociation/coordination scenario or inversion process involving the coordinated MeS moiety. (b) For a recent report describing the facile non-dissociative inversion of a MeTe ligand at an osmium cluster, see: Shim, E. K. S.; Leong, W. K.; Li, Y.-Z.; Richmond, M. G. Isomerization of the osmium–tellurium cluster $Os_3(\mu\text{-}TeR)_2(CO)_{10}$: a kinetic and computational study. *Dalton Trans.* **2016**, *45*, 7158.

(18) Epimers are a class of stereoisomers best viewed as diastereomers that differ in configuration at one stereocenter. See: Eliel, E. L.; Wilen, S. H.; Doyle, M. P. *Basic Organic Stereochemistry*. Wiley-Interscience, New York, 2001.

(19) In determining the number of possible bridging isomers, we only considered those isomers with mutually syn sites given the short bite angle of the PS ligand that precludes the coordination of trans equatorial-equatorial and trans axial-equatorial sites.

(20) The true total of isomers in $H_2Ru_3(CO)_7(PS)(\mu_3\text{-}S)$ is estimated to be forty-two, excluding mirror images. Twelve additional isomers can

be added to the quoted total of thirty isomers if one includes the bridging of ruthenium centers through the axial and remote equatorial sites across the Ru-Ru bond. However, these isomers lie > 25 kcal/mol above **C2** and are not energetically competitive with the thirty isomers displayed in Figure 3.

(21) (a) The endo addition of the MeS donor to give the κ^1-SP analogue of **D** was computationally evaluated and the corresponding MeS-addition transition structure (**TSABD_alt**) was found to lie 2.1 kcal/mol higher in energy (ΔG) than **TSABD**. (b) We also examined the addition of both donor groups to the ruthenium atom that is bridged by both hydrides and confirm the failure of an exo approach by the PS ligand. Here the incoming ligand reorients itself and adds to the ruthenium center in an endo fashion in a trajectory that is opposite the capping sulfido moiety. The computed energies for **TSABD_endo_alt1** (Me_2P addition) and **TSABD_endo_alt2** (MeS addition) lie 5.4 and 5.7 kcal/mol, respectively, above **TSABD**. Collectively, these additional calculations reinforce a regiospecific reaction that favors the addition of the Me_2P donor to a ruthenium center in cluster **1** that contains a single edge-bridging hydride. (c) The alternative exo addition of the PS donor to the ruthenium center (**TSABD_exo**) was also examined and confirmed to lie 1.4 kcal/mol above **TSABD**.

(22) (a) The vertex expansion computed for cluster **1** on the addition of the PS ligand is consistent with Polyhedral Skeletal Electron Pair (PSEP) Theory which predicts the opening of the *nido* frame containing 6 skelelal electron pairs (SEP) to an *arachno* geometry in the addition adduct that contains 7 SEP. (b) For a detailed discussion on the theoretic underpinnings for PSEP Theory, see: Mingos, D. M. P.; Wales, D. J. *Introduction to Cluster Chemistry*, Prentice Hall, Englewood Cliffs, New Jersey, 1990.

(23) For reviews on this concept, see: (a) Vahrenkamp, H. What Do We Know about the Metal-Metal Bond? *Angew. Chem. Int. Ed. Engl.* **1978**, *17*, 379. (b) Adams, R. D.; Horváth, I. T. Novel Reactions of Metal Carbonyl Cluster Compounds. *Prog. Inorg. Chem.* **1985**, *33*, 127. (c) Darensbourg, D. L. *Ligand Substitution Reactions in The Chemistry of Metal Cluster Complexes*. Shriver, D. F.; Kaesz, H. D.; Adams, R. D. eds. VCH Publishers, New York, 1990, Chap. 4.

(24) Planalp, R. P.; Vahrenkamp, H. Reversible Metal-Metal Bond Cleavage in $FeCo_2$ and FeCoW Clusters. *Organometallics* **1987**, *6*, 492.

(25) See also: Huttner, G.; Schneider, J.; Muller, H. D.; Mohr, G.; van Seyerl, J.; Wohlfahrt, L. Reversible Opening of a Trinuclear Heterometal Cluster. *Angew. Chem. Int. Engl.* **1979**, *18*, 76.

(26) For examples of hydride fluxionality in metal cluster compounds, see: (a) Alvarez, A. M.; Garcia, E. M.; Garcia-Vivo, Daniel; Ruiz, M. A.; Toyos, A. Structure and dynamics of heterometallic clusters derived from addition of metal carbonyl fragments to the unsaturated hydride $[W_2Cp_2(\mu\text{-H})(\mu\text{-PPh}_2)(NO)_2]$. *Dalton Trans.* **2017**, *46*, 15317. (b) Tahara, A.; Kajigaya, M.; Takao, T.; Suzuki, H. Synthesis and dynamic properties of a triruthenium complex containing μ_3-η^2(∥)-ethyne and μ_3-methylidyne ligands: equilibrium of an ethyne-hydrido complex with a nonclassical μ_3-vinyl complex. *Organometallics 2013*, **32**, 260. (c) Skinner, D. M.; Rosenberg, E.; Bracker-Novak, J.; Aime, S.; Osella, D.; Gobetto, R.; Milone, L. Carbon-metal hydrogen interchange in organometal clusters of ruthenium and osmium. *Organometallics* **1988**, *7*, 856. (d) Adams, R. D.; Captain, B.; Smith, M. D.; Beddie, C.; Hall, M. B. Unsaturated Platinum - Rhenium Cluster Complexes. Synthesis, Structures and Reactivity. *J. Am. Chem. Soc.* **2007**, *129*, 5981. (e) Jiménez, M. V.; Lahoz, F. J.; Lukesšová, L.; Miranda, J. R.; Modrego, F. J.; Nguyen, D. H.; Oro, L. A.; Pérez-Torrente, J. J. Hydride Mobility in Trinuclear Sulfido Clusters with the Core $[Rh_3(\mu\text{-H})(\mu_3\text{-S})_2]$: Molecular Models for Hydrogen Migration on Metal Sulfide Hydrotreating Catalysts. *Chem. Eur. J.* **2011**, *17*, 8115.

(27) (a) The van der Waals radii for hydrogen, carbon, and phosphorus are 1.20 Å, 1.70 Å, and 1.80 Å, respectively, which places the internuclear contact of the terminal Ru-H group and the adjacent Me_2P moiety at the outermost most boundary for covalent interaction between the H, C, and P atoms. (b) The atomic radii were taken from the available periodic table of elements on the Los Alamos National Laboratory (LANL) site: http://periodic.lanl.gov/1.shtml.

(28) For an excellent treatise on the bonding of bridging hydrides in organometallic compounds, see: Parkin, G. Metal-Metal Bonding in Bridging Hydride and Alkyl Compounds. *Struct. Bond.* **2010**, *136*, 113.

(29) For other cluster examples that exhibit a low-energy tripodal exchange of groups at a metal cluster, see: (a) Begum, S. A.; Chowdhury, M. A. H.; Ghosh, S.; Tocher, D. A.; Yang, L.; Richmond, M. G.; Hardcastle, K. I.; Rosenberg, E.; Kabir, S. E. Experimental and computational preference for phosphine regioselectivity and stereoselective tripodal rotation in $HOs_3(CO)_8(PPh_3)_2(\mu\text{-}1,2\text{-}\eta^1,\kappa^1\text{-}C_7H_4NS)$. *RSC Adv.* **2018**, *8*, 32672. (b) Adams, R. D.; Chen, M.; Elpitiya, G.; Zhang, Q. Synthesis and Characterizations of Bismuth-Bridged Triiridium Carbonyl Complexes Containing Germyl/Germylene and Stannyl/Stannylene Ligands. *Organometallics* **2012**, *31*, 7264.

(30) Species **I** serves as a suitable precursor for the resting state κ^1-PS intermediate observed by NMR spectroscopy. Hydride migration from the remote Ru-Ru bond to the P-substituted ruthenium atom, coupled with a tripodal rotation of the $P_{eq} \rightarrow P_{ax}$ position would generate an intermediate with C_s symmetry (see below). Alternatively, tripodal rotation of the three groups at the P-substituted ruthenium center, followed by hydride migration, would also produce the κ^1-PS intermediate.

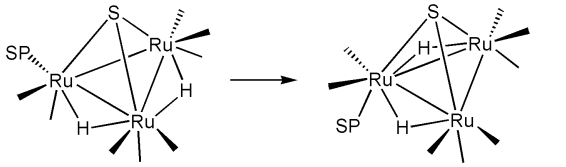

species I NMR observed κ^1 isomer

(31) For DFT results on the pyramidalization of MeS groups in the sulfide-bridged dimer $Fe_2(CO)_6(\mu\text{-SMe})_2$, see: In-noi, K.; Haller, K. J.; Hall, G. B.; Brezinski, W. P.; Marx, J. M.; Sakamoto, T.; Evans, D. H.; Glass, R. S.; Lichtenberger, D. L. Spectroscopic and Computational Study of Bis(μ-methylthiolato)diironhexacarbonyl: Homoassociative Stabilization of the Dianion and a Chemically Reversible Reduction/Reoxidation Cycle. *Organometallics* **2014**, *33*, 5009.

(32) Capellos, C.; Bielski, B. H. J. *Kinetic Systems: Mathematical Description of Chemical Kinetics in Solution*. Robert E. Krieger Publishing Co., Huntington, NY, 1980.

(33) For other notable examples of organometallic/inorganic reactions whose rates to equilibrium have been kinetically investigated, see: (a) Caulton, K. G.; Chisholm, M. H.; Streib, W. E.; Xue, Z. Direct Observation of α-Hydrogen Transfer from Alkyl to Alkylidyne Ligands in $(Me_3CCH_2)_3W{:}CSiMe_3$. Kinetic and Mechanistic Studies of Alkyl-Alkylidyne Exchange. *J. Am. Chem. Soc.* **1991**, *113*, 6082. (b) Gavriluta, A.; Buchel, G. E.; Freitag, L.; Novitchi, G.; Tommasino, J. B.; Jeanneau, E.; Kuhn, P.-S.; Gonzalez, L.; Arion, V. B.; Luneau, D. Mechanism Elucidation of the cis-trans Isomerization of an Azole Ruthenium-Nitrosyl Complex and Its Osmium Counterpart. *Inorg. Chem.* **2013**, *52*, 6260. (c) Leal, B. C.; Aydos, G. L. P.; Netz, P. A.; Dupont, J. Ru-Catalyzed Estragole Isomerization under Homogeneous and Ionic Liquid Biphasic Conditions. *ACS Omega* **2017**, *2*, 1146. (d) Kobayashi, K.; Satsu, Y.; Hoshino, Y.; Arai, S.; Hatkeyama, K.; Endo, A.; Shimizu, K.; Sato, G. P. Faciala-Meridional Isomerization of Some Tris-(β-diketonato)ruthenium(III) Complexes. *Bull. Chem. Soc. Jpn.* **1989**, *62*, 3252. (e) Hunter, S. S. C.; Chen, S.-J.; Steren, C. A.; Richmond, M. G.; Xue, Z.-L. Syntheses and Characterization of Tantalum Alkyl Imides and Amide Imides. DFT Studies of Unusual α-$SiMe_3$ Abstraction by an Amide Ligand. *Organometallics* **2015**, *34*, 5687.

(34) We also investigated the tripodal rotation in species **C9**, the isomer produced by migration of the hydride (H) syn to the Me_2P moiety in **C1** to the free Ru-Ru bond. Rotation of the three ligands at the

Ru(CO)(κ^2-PS) center in **C9** promoted the migration of the hydride (H-red) syn to the MeS ligand to the free Ru-Ru bond with the formation of **C11** as depicted below. Despite several attempts to model the tripodal rotation in **C9**, we were not successful and terminated this line of study.

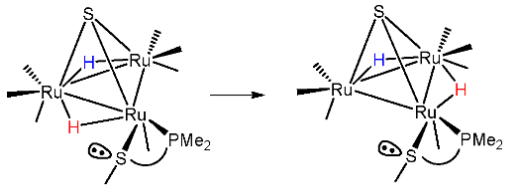

(35) Bruce, M. I.; Jensen, C. M.; Jones, N. L. *Inorg. Synth.* **1989**, *26*, 259.
(36) Cresswell, T. A.; Howard, J. A. K.; Kennedy, F. G.; Knox, S. A. R.; Wadepohl, H. Organosulphur-Transition-metal Chemistry. Part 5. Face Bonding of Cycloheptatrienyl and Cyclo-octatetraene Ligands in Sulphur-Ruthenium Clusters: Crystal and Molecular Structure of $[Ru_3(CO)_6(\mu_3\text{-}SBu^t)\{\mu_3\text{-}(\eta_7\text{-}C_7H_7)\}]$. *Dalton Trans.* **1981**, 2220.
(37) Reinius, H. K.; Laitinen, R. H.; Krause, A. O. I.; Pursiainen, J. T. Hydroformylation of methyl methacrylate with heterodonor phosphine rhodium catalysts prepared in situ. *Catal. Lett.* **1999**, *60*, 65.
(38) Sheldrick, G. M. SHELXT--Integrated space-group and crystal structure determination. *Acta Cryst.* **2015**, *A71*, 3.
(39) Sheldrick, G. M. Crystal structure refinement with SHELXL. *Acta Cryst.* **2015**, *C71*, 3.
(40) Spek, A. L. Structure validation in chemical crystallography. *Acta Cryst.* **2009**, *D65*, 148.
(41) Dolomanov, O. V.; Bourhis, L. J.; Gildea, R. J.; Howard, J. A. K.; Puschmann, H. OLEX2: a complete structure solution, refinement and analysis program. *J. Appl. Cryst.* **2009**, *42*, 339.
(42) Frisch, M. J., *et al.* Gaussian 09, Revision E.01; Gaussian, Inc. Wallingford, CT, USA, 2009.
(43) Tao, J.; Perdew, J. P.; Staroverov, V. N.; Scuseria, G. E. Climbing the Density Functional Ladder: Nonempirical Meta–Generalized Gradient Approximation Designed for Molecules and Solids. *Phys. Rev. Lett.* **2003**, *91*, 146401.
(44) Andrae, D.; Haeussermann, U.; Dolg, M.; Stoll, H.; Preuss, H. Energy-adjusted *ab initio* pseudopotentials for the second and third row transition elements: Molecular test for M_2 (M=Ag, Au) and MH (M=Ru, Os). *Theor. Chim. Acta* **1990**, *77*, 123.
(45) (a) Petersson, G. A.; Bennett, A.; Tensfeldt, T. G.; Al-Laham, M. A.; Shirley, W. A.; Mantzaris, J. A complete basis set model chemistry. I. The total energies of closed-shell atoms and hydrides of the first-row elements. *J. Chem. Phys.* **1988**, *89*, 2193. (b) Petersson, G. A.; Al-Laham, M. A. A complete basis set model chemistry. II. Open-shell systems and the total energies of the first-row atoms. *J. Chem. Phys.* **1991**, *94*, 6081.
(46) Cramer, C. J. *Essentials of Computational Chemistry*, 2nd ed.; Wiley: Chichester, UK, 2004; pp 378-379.
(47) (a) Hall, M. B.; Fenske, R. F. Electronic Structure and Bonding in Methyl- and Perfluoromethyl(pentacarbonyl)manganese. *Inorg. Chem.* **1972**, *11*, 768. (b) Manson, J.; Webster, C. E.; Hall, M. B. *JIMP2*; Texas A&M University, College Station, TX, USA, 2006; http://www.chem.tamu.edu/jimp2/index.html.
(48) Carpenter, B. K. *Determination of Organic Reaction Mechanisms*. Wiley-Interscience: New York, 1984.

Table of Contents Picture